2015

Magnetism of Ta dichalcogenide monolayers tuned by strain and hydrogenation

Priyanka Manchanda
University of Nebraska-Lincoln, priyanka.manchanda@vanderbilt.edu

Vinit Sharma
University of Connecticut - Storrs

Hongbin Yu
Arizona State University

David J. Sellmyer
University of Nebraska-Lincoln, dsellmyer@unl.edu

Ralph A. Skomski
University of Nebraska-Lincoln, rskomski2@unl.edu

Magnetism of Ta dichalcogenide monolayers tuned by strain and hydrogenation

Priyanka Manchanda,[1] Vinit Sharma,[2] Hongbin Yu,[3] D. J. Sellmyer,[1] and Ralph Skomski[1]
[1]*Department of Physics and Astronomy and Nebraska Center for Materials and Nanoscience, University of Nebraska, Lincoln, Nebraska 68588, USA*
[2]*Department of Materials Science and Engineering and Institute of Materials Science, University of Connecticut, Storrs, Connecticut 06269, USA*
[3]*School of Electrical, Computer, and Energy Engineering, Arizona State University, Tempe, Arizona 85287, USA*

(Received 22 May 2015; accepted 12 July 2015; published online 21 July 2015)

The effects of strain and hydrogenation on the electronic, magnetic, and optical properties of monolayers of Ta based dichalcogenides (TaX_2; $X = S$, Se, and Te) are investigated using density-functional theory. We predict a complex scenario of strain-dependent magnetic phase transitions involving paramagnetic, ferromagnetic, and modulated antiferromagnetic states. Covering one of the two chalcogenide surfaces with hydrogen switches the antiferromagnetic/nonmagnetic TaX_2 monolayers to a semiconductor, and the optical behavior strongly depends on strain and hydrogenation. Our research opens pathways towards the manipulation of magnetic as well as optical properties for future spintronics and optoelectronics applications. © *2015 AIP Publishing LLC*.
[http://dx.doi.org/10.1063/1.4927286]

Two-dimensional transition-metal dichalcogenides (2D TMDs) combine many advantages of graphene and conventional thin-film materials and have recently attracted much attention as potential materials for electronics, photovoltaic cells, sensors, catalysis, and energy storage.[1–8] Examples are flexible electronic devices, beyond-graphene nanoelectronics such as thin-film transistors,[6] and transition-metal disulfide thin films in water electrolysis for hydrogen production.[3] Compared to graphene, which needs large strain to open a band gap,[9,10] the electronic properties of 2D TMDs are very versatile. Among these features are direct band gaps in the visible wavelength range, excellent room-temperature electron mobility, mechanical properties, and easy chemical functionalization.[1–4] The exploration of these two-dimensional materials is an important aspect of current research in nanoelectronics and other areas, as exemplified by efforts to approach the ultimate limits of thin-film transistor technology.[6,7]

Thin films of TMDs, such as MoS_2, WS_2, $MoSe_2$, and $TaSe_2$, exhibit excellent "peel-off" characteristics and can be easily synthesized, using methods such as chemical, liquid, and micromechanical exfoliation techniques and chemical vapor deposition.[11–13] A related advantage of the films is their mechanical robustness, and experiment shows that 2D TMDs can sustain strain of up to about 11%.[14] The properties of 2D TMDs vary from semiconducting (MoS_2, WS_2) to metallic ($NbSe_2$, TaS_2) and magnetic (VS_2, VSe_2).[15–18] Very recently, it has become clear that 2D TMDs exhibit striking physical-property changes due to strain,[14,19–27] chemical functionalization,[28–33] doping with transition metals,[34] and external electric fields.[35] For instance, it has been demonstrated experimentally that strain modulates the bandgap of monolayers and bilayers in MoS_2.[19] Density-functional theory (DFT) play an important role in the prediction and investigation of the properties of these materials. Examples are the strong effect of uniaxial and isotropic strains on the electronic properties of early MX_2 monolayers ($M = Sc$, Ti, Zr, Hf, Ta, Cr; $X = S$, Se, Te),[20] strain-induced bandgap changes in MoS_2,[21] and semiconductor-to-metal transitions in $SnSe_2$.[22]

An emerging topic in 2D TMD research is the investigation of *magnetic* degrees of freedom. Magnetic effects are important by themselves, due to potential applications in spin electronics and because they are coupled with other physical phenomena such as electrical conductivity. This research is exemplified by calculations of the magnetic moment for different chemical compositions[20] and of strain-induced magnetism.[23–25] Some of the published information is contradictory such as the reports of strain-dependent ferromagnetism[26] and antiferromagnetism[27] in NbX_2 ($X = S$, Se) monolayers.

Chemical functionalization is another approach to modify magnetic properties. Electronic-structure calculations suggest that adsorbed hydrogen molecules dissociate at the TMD surface, each hydrogen forming a bond with a chalcogen.[29] In VX_2 monolayers ($X = S$, Se, and Te), various states have been predicted for different hydrogen coverages.[30] Some combined effects have also been studied, such as ferromagnetism in MoS_2,[31] and various electronic phases in VX_2 ($X = S$, Se, Te)[32] caused by strain and hydrogenation. Experimentally, adsorbed fluorine has been shown very recently to create a small magnetic moment of 0.06 emu/g in MoS_2 nanosheets.[33]

This letter focus on tantalum dichalcogenides TaS_2, $TaSe_2$, and $TaTe_2$ monolayers. We use first-principles calculations to explore the strain and hydrogenation effects on the electronic, magnetic, and optical properties of these materials and predict a complex scenario of magnetic and nonmagnetic phase transitions. From the viewpoint of electron transport, the transitions involve metallic and "semimetallic"

states and direct and indirect semiconductivity, whereas the magnetic phases include paramagnets, ferromagnets, and modulated antiferromagnets.

Our DFT calculations are performed using the projector augmented wave (PAW) method,[36] as implemented in the Vienna *ab-initio* simulation package (VASP).[37,38] Within the generalized gradient approximation (GGA), we employ Perdew-Burke-Ernzerhof (PBE) exchange and correlation functionals.[39] The kinetic energy cutoff of plane-wave expansion is taken as 520 eV. All the geometric structures are fully relaxed until the force on each atom is less than 0.002 eV/Å, and the energy-convergence criterion is 1×10^{-6} eV. For the electronic-structure calculations, a $23 \times 23 \times 1$ k-point grid is used. To investigate the spin structure, we construct a $4 \times 4 \times 1$ supercell, and a sufficiently large vacuum is used in the vertical direction to avoid the interaction between neighboring supercells. Figures 1(a) and 1(e) show the top and side views of the monolayers, respectively. The big red arrows in (a) show the positive isotropic strain to which the monolayers are subjected.

The structural relaxation is described in the supplementary material.[40] To study the magnetic order, we have considered four different spin configurations, namely, paramagnetic (PM), ferromagnetic (FM), and two antiferromagnetic (AFM and AFM′) spin structures, the AFM′ structure as previously[27] suggested. Figures 1(a)–1(d) show these spin configurations. In unstrained $TaTe_2$, the AFM state has the lowest energy, whereas unstrained TaS_2 and $TaSe_2$ are paramagnetic.

Figure 2(a) displays the strain dependence of the energies of the magnetically ordered spin configurations of

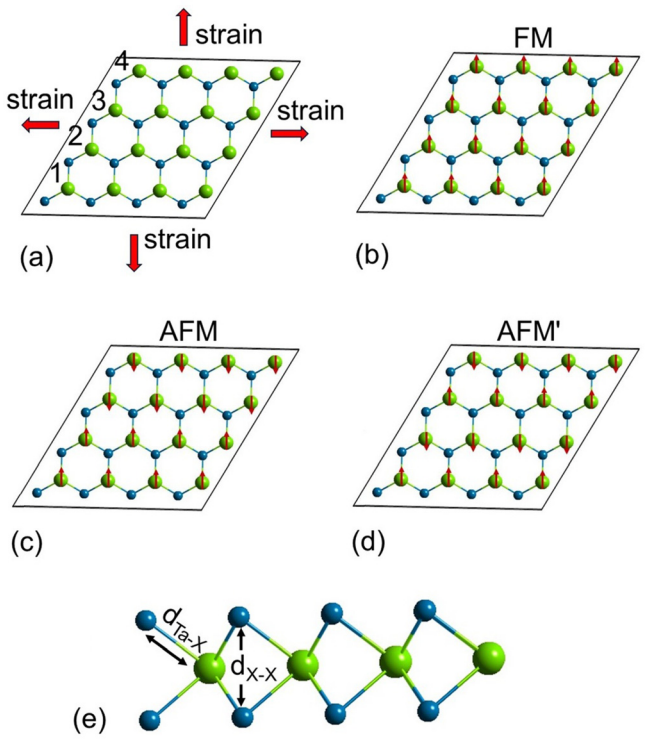

FIG. 1. (a) Top view of 4×4 TaX_2 supercell (X = S, Se, and Te) subjected to isotropic strain, (b) FM spin configuration, (c) AFM spin configuration, with ↑ electrons in rows 1 and 2 and ↓ electrons in rows 3 and 4, (d) AFM′ spin configuration, with ↑ electrons in rows 1 and 3 and ↓ electrons in 2 and 4, and (e) side view of TaX_2 supercell. Green and blue colors are used for Ta and X atoms, respectively.

$TaTe_2$ relative to the paramagnetic energy E_{PM}. In $TaTe_2$, the AFM state remains stable up to an isotropic strain of 2%. Above 2%, the magnetic order is ferromagnetic. The PM and AFM′ have the same energy, meaning that the AFM' state degenerates into the PM state with zero Ta atomic moments.

Figure 2(b) shows the strain dependence of the atomic magnetic moments in the monolayers. In $TaTe_2$, the atomic moments corresponds to the AFM state for small strain and to the FM state for strains larger than 2%. In TaS_2 and $TaSe_2$, all nonzero moments are FM. In all cases, the atomic magnetic moments increase with increasing strain. For example, in $TaTe_2$, strains of 4% and 10% yield ferromagnetic moments of 0.28 μ_B and 0.57 μ_B per Ta atom, respectively. The inset of Fig. 2(b) plots the magnetic moments of the Ta atoms in the AFM spin configuration, Ta-1 and Ta-2 corresponding to rows 1 and 2 in Fig. 1(a), respectively. The Ta moments in unstrained $TaTe_2$, 0.15 μ_B (Ta-1) and 0.36 μ_B (Ta-2), are different, in spite of the structural equivalence of the two sites. This modulation, not shown in the schematic spin structure of Fig. 1(c), is reminiscent of spin-density waves in Cr and of heavy rare earths below room temperature.

To check the robustness of our DFT calculations with respect to the exchange-correlation potential, we have compared our original GGA-PBE findings with a modified PBE (PBEsol) potential. The latter limit is specifically adapted to surfaces of very dense (highly compressed) solids[41] and not actually realized in the present films, but it yields similar results. The spin structure remains unchanged, including the $TaTe_2$ FM-AFM transition at about 2% strain, whereas the magnetic moment is reduced by about 7%, for example, from 0.56 to 0.52 μ_B per Ta atom in 10%-strained $TaTe_2$.

In contrast to $TaTe_2$, unstrained TaS_2 and $TaSe_2$ monolayers remain paramagnetic below about 6% strain. At about 6% strain, both TaS_2 and $TaSe_2$ become ferromagnetic with respective magnetic moments of 0.24 μ_B and 0.34 μ_B per Ta atom. The magnetic moment mainly arises from Ta atoms and the contribution of S, Se, and Te to the total magnetic moment is negligible. The moment increases with strain, and at 10%, it reaches 0.48 μ_B and 0.50 μ_B for TaS_2 and $TaSe_2$, respectively. Figure 3 shows the 5d DOS of TaS_2 and $TaSe_2$ for unstrained monolayers and for a strain of 6%. We see that the magnetic moment arises from Ta 5d states near the Fermi level, whose spin degeneracy is lifted by the strain. The character of these states is predominantly of the $|m| = 2$ type, comprising the $d_{x^2-y^2}$ and d_{xy} orbitals, which lie in the film plane. In contrast to graphene, there is also some admixture of $|m| = 1$ character at the Fermi level, especially d_{xz}, because the chalcogen atoms are located slightly above and below the Ta plane, as shown in Fig. 1(e).

Due to its transition from antiferromagnetism to ferromagnetism, the DOS of $TaTe_2$ requires a separate consideration. Figures 4(a) and 4(b) show the spin-polarized local d-DOS of the Ta-1 and Ta-2 atoms in the unstrained AFM state. The exchange splitting of Ta-2 is larger than that of Ta-1, which corresponds to the different moments described above.

Hydrogen adsorption drastically affects the properties of some 2D TMDs. We consider the electronic properties of hydrogenated-TaX_2 with one surface covered by hydrogen

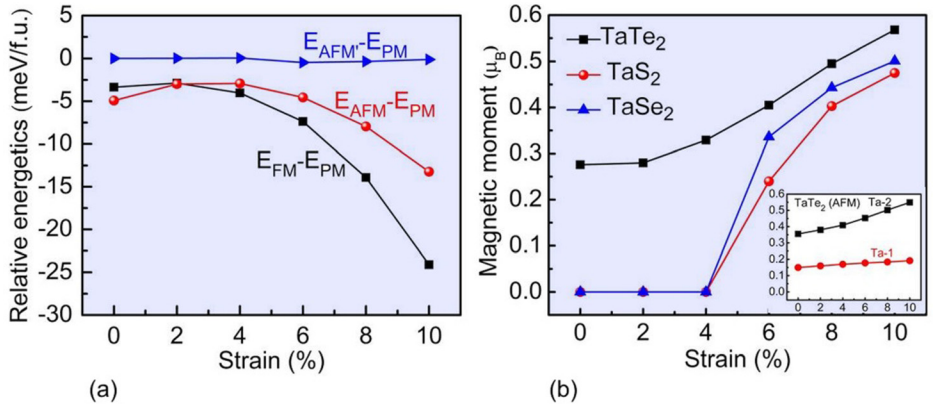

FIG. 2. Spin structure and magnetization of TaX_2 monolayers: (a) energies of the FM, AFM, and AFM' states of $TaTe_2$ relative to the PM state and (b) atomic moment, measured in μ_B per Ta atom. The inset shows the magnetic moment of the Ta-1 and Ta-2 atoms in the AFM spin configuration of Fig. 1(a).

atoms (TaX_2-1H). Figure 5(a) shows a perspective view of the corresponding structure, where we follow the previous research[29,31] by assuming that the most stable hydrogen location is on top of the X atoms. Our calculations show that the optimized lattice constants of TaX_2-1H are expanded by 1.5%–3.5% compared to TaX_2, reaching 3.39 Å, 3.48 Å, and 3.82 Å for TaS_2-1H, $TaSe_2$-1H, and $TaTe_2$-1H, respectively. For S-H, Se-H, and Te-H, the respective bond lengths are 1.37 Å, 1.51 Å, and 1.71 Å.

The hydrogenation strongly affects the electronic properties of the monolayers. Figures 5(b)–5(d) show the calculated band structures of TaS_2-1H, $TaSe_2$-1H, and $TaTe_2$-1H. In contrast to the hydrogen-free monolayers, which exhibit both ↑ and ↓ states at the Fermi level (Figs. 3 and 4), there are no states at the Fermi level of the hydrogenated systems. This means that the hydrogenated Ta monolayers are semiconducting. From Fig. 5, we see that TaS_2-1H and $TaSe_2$-1H have indirect band gaps of about 0.75 eV and 0.67 eV, respectively, whereas $TaTe_2$-1H exhibits a direct band gap of 0.62 eV. The transition from antiferromagnetic or paramagnetic metallicity to semiconducting behavior occurs because the hydrogen donates electrons that fill the empty Ta 5d-states just above the Fermi level, which is similar to the situation in VX_2 monolayers.[30]

Figure 5 shows that hydrogenation causes the top of the occupied band, located at the K point, is very close to the Fermi level. For incomplete hydrogen coverage, where the Fermi level is somewhat lower, band-filling arguments suggest zero-temperature conductivity reminiscent of semimetals. A complicating factor is that the hole carriers move in a two-dimensional environment and are therefore subject to weak localization[42] near hydrogen vacancies.

Our research shows that TaX_2 is a particularly interesting and versatile 2D TMD system, especially with respect to strain and hydrogenation. It is instructive to compare the present findings with the earlier research on MX_2 thin films. Strain-induced magnetism in TMD monolayers has been

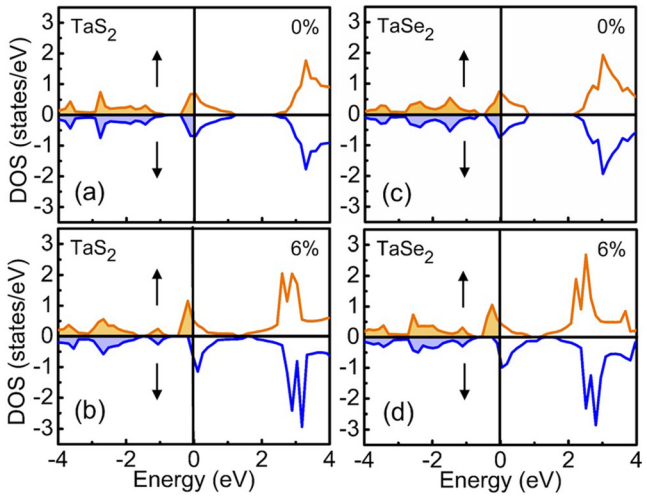

FIG. 3. Spin-polarized partial 5d-(DOS) of unstrained and 6% strained monolayers: ((a) and (b)) TaS_2 and ((c) and (d)) $TaSe_2$.

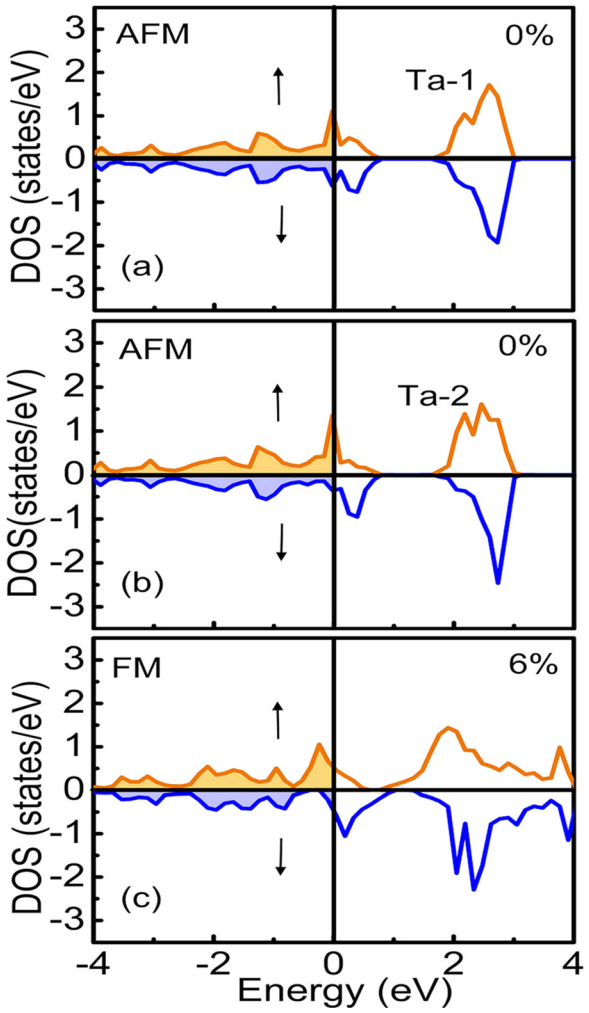

FIG. 4. Spin-polarized partial 5d-DOS: ((a) and (b)) unstrained AFM state of $TaTe_2$ and (c) FM state with 6% strain of $TaTe_2$.

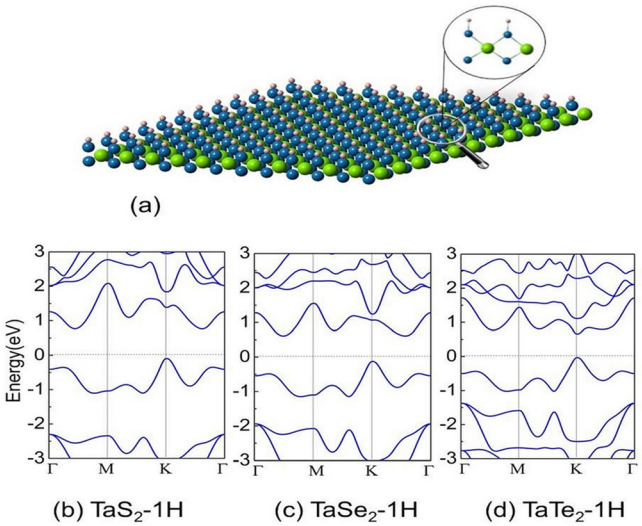

FIG. 5. Hydrogenated TaX_2 monolayers: (a) monolayer with one side fully covered with hydrogen atoms (green: Ta, blue: X, and gray: H), (b) band structure of TaS_2-1H, (c) band structure of $TaSe_2$-1H, and (d) band structure of $TaTe_2$-1H.

ascribed to the competition between covalent-bond and ionic-bond interactions.[25,26] In fact, neither covalent-bond nor the ionic-bond interactions are likely to change very much due to strain. Our explanation is slightly different, namely, a Stoner transition caused by band narrowing, which is only loosely related to ionicity.[43]

Similar arguments apply to the occurrence of AFM order. Antiferromagnetism in *unstrained* $TaTe_2$ has been explained as a superexchange mechanism,[27,30] but as in the FM case, the AFM can also be explained in terms of the band structure, as itinerant antiferromagnetism mediated by chalcogen atoms. In fact, a previous calculation,[20] dealing with unstrained $TaTe_2$, suggests that the monolayer is actually *ferromagnetic* rather than antiferromagnetic. This finding is obtained by comparing the FM energy with the AFM′ energy, while the AFM state was not considered. Our calculations safely exclude a FM ground state and show that the ground state is more complicated than simple antiferromagnetism.

Much of the developing interest in these materials derives from their electric and optical properties.[44] These properties are particularly versatile in the Ta dichalcogenides, with transitions triggered by strain and hydrogenation. Optical and electric-transport properties derive from the dielectric susceptibility $\varepsilon(\omega) = \varepsilon'(\omega) + i\varepsilon''(\omega)$. To calculate the effect of interband transitions on the respective real and imaginary parts $\varepsilon'(\omega)$ and $\varepsilon''(\omega)$, we have used the PAW formalism.[45] Figure 6 shows the calculated absorption index $\kappa = n''$, that is, the imaginary part of the index of refraction, for the ferromagnetic metallic $TaTe_2$ film with 6% strain. The absorption index has been determined from[46]

$$\kappa = \frac{1}{\sqrt{2}}\sqrt{\left(\varepsilon'^2 + \varepsilon''^2\right)^{1/2} - \varepsilon'}. \quad (1)$$

There is a big absorption peak near 2.2 eV, that is, in the middle of the *green* color range. The peak is caused by transitions from the occupied band just below the Fermi level to the unoccupied band slightly above 2 eV (Fig. 4(c)). The

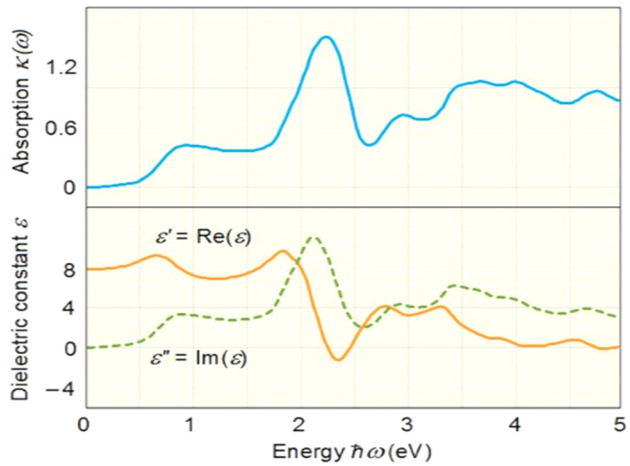

FIG. 6. Dielectric constant $\varepsilon(\omega)$ and absorption index for $TaTe_2$ with 6% strain. The electric field is in the plane, in the x-direction.

TaS_2 film with 6% strain has an absorption peak in the blue range (Fig. 3(b)), and in both cases, the peaks move towards lower frequencies as the strain increases. Hydrogenation further reduces the frequency, down towards infrared for $TaTe_2$-1H.

Our optical analysis confirms the unprecedented versatility of Ta dichalcogenide thin films, but further research is necessary to fully understand and exploit the potential of the films. For example, the conductivity $\sigma(\omega) = \sigma(\omega) = \sigma_o + i\omega\varepsilon(\omega)$ covers a wide range from insulators and semiconductors to metals, which is beneficial for electronics applications, but additional mean-free-path considerations are needed to cover the interesting low-frequency range. Excitonic and other correlations effects are also important, especially in the insulating and semiconducting films,[47] and likely to enhance the absorption at lower frequencies.

In conclusion, we have used DFT calculations to study the electronic, magnetic, and optical properties of strained and hydrogenated Ta dichalcogenide monolayers and to show that these films exhibit an extraordinary versatility. Unstrained TaS_2 and $TaSe_2$ are Pauli-paramagnetic, but both become ferromagnetic at a strain of about 6%. For unstrained $TaTe_2$, we find a complicated antiferromagnetic spin structure that changes to ferromagnetic above 2% strain. Hydrogenation changes the metallic TaX_2 monolayers to direct or indirect semiconductors, and optical properties are also affected by strain and hydrogenation. While there remain challenges to future theoretical and experimental research, we expect this intriguing class of materials to play an important role in the quest for materials beyond graphene.

The authors are grateful to A. Kashyap, S. S. Jaswal, S. Auluck, and P. A. Dowben for discussing various details. This work has been supported by ARO (W911NF-10-2-0099 (P.M.)), DOE BES (DE-FG02-04ER46152 (R.S. and D.J.S.)), Holland Computing Center, and NCMN.

[1]M. Chhowalla, H. S. Shin, G. Eda, L.-J. Li, K. P. Loh, and H. Chang, Nat. Chem. **5**, 263 (2013).
[2]B. Radisavljeic, A. Radenovic, J. Brivio, V. Giacometti, and A. Kis, Nat. Nanotechnol. **6**, 147 (2011).
[3]H. Pan, Sci. Rep. **4**, 5348 (2014).

[4]Z. Gong, G.-B. Liu, H. Yu, D. Xiao, X. Cui, X. Xu, and W. Yao, Nat. Commun. **4**, 2053 (2013).
[5]S. Das, R. Gulotty, A. V. Sumant, and A. Roelofs, Nano Lett. **14**, 2861 (2014).
[6]T. Palacios, Nat. Nanotechnol. **6**, 464 (2011).
[7]R. F. Service, Science **348**, 490 (2015).
[8]H. L. Zhuang and R. G. Hennig, J. Phys. Chem. C **117**, 20440 (2013).
[9]V. M. Pereira, A. H. Castro Neto, and N. M. R. Peres, Phys. Bev. B **80**, 045401 (2009).
[10]P. Kumar, R. Skomski, P. Manchanda, A. Kashyap, and P. A. Dowben, Curr. Appl. Phys. **14**, S136 (2014).
[11]J. N. Coleman, M. Lotya, A. O'Neill, S. D. Bergin, P. J. King, U. Khan, K. Young, A. Gaucher, S. De, R. J. Smith *et al.*, Science **331**, 568 (2011).
[12]R. J. Smith, P. J. King, M. Lotya, C. Wirtz, U. Khan, S. De, A. O'Neill, G. S. Duesberg, J. C. Grunlan, G. Moriarty *et al.*, Adv. Mater. **23**, 3944 (2011).
[13]X. Zhang and Y. Xie, Chem. Soc. Rev. **42**, 8187 (2013).
[14]S. Bertolazzi, J. Brivio, and A. Kis, ACS Nano **5**, 9703 (2011).
[15]A. Kuc, N. Zibouche, and T. Heine, Phys. Rev. B **83**, 245213 (2011).
[16]Z. Y. Zhu, Y. C. Cheng, and U. Schwingenschlögl, Phys. Rev. B **84**, 153402 (2011).
[17]Y. Ding, Y. L. Wang, J. Ni, L. Shi, S. Q. Shi, and W. H. Tang, Physica B **406**, 2254 (2011).
[18]C. Ataca, H. Şahin, and S. Ciraci, J. Phys. Chem. C **116**, 8983 (2012).
[19]H. J. Conley, B. Wang, J. I. Ziegler, R. F. Haglund, S. T. Pantelides, and K. I. Bolotin, Nano Lett. **13**, 3626 (2013).
[20]H. Guo, N. Lu, L. Wang, X. Wu, and X. C. Zeng, J. Phys. Chem. C **118**, 7242 (2014).
[21]Q. Yue, J. Kang, Z. Shao, X. Zhang, S. Chang, G. Wang, S. Qin, and J. Li, Phys. Lett. A **376**, 1166 (2012).
[22]Y. Huang, C. Ling, H. Liu, S. Wang, and B. Geng, J. Phys. Chem. C **118**, 9251 (2014).
[23]H. Zheng, B. Yang, D. Wang, R. Han, X. Du, and Y. Yan, Appl. Phys. Lett. **104**, 132403 (2014).
[24]L. Kou, C. Tang, Y. Zhang, T. Heine, C. Chen, and T. Frauenheim, J. Phys. Chem. Lett. **3**, 2934 (2012).
[25]Y. Ma, Y. Dai, M. Guo, C. Niu, Y. Zhu, and B. Huang, ACS Nano **6**, 1695 (2012).
[26]Y. Zhou, Z. Wang, P. Yang, X. Zu, L. Yang, X. Sun, and F. Gao, ACS Nano **6**, 9727 (2012).
[27]Y. Xu, X. Liu, and W. Guo, Nanoscale **6**, 12929 (2014).
[28]D. Voiry, A. Goswami, R. Kappera, C. Silva, D. Kaplan, T. Fujita, M. Chen, T. Asefa, and M. Chhowalla, Nat. Chem. **7**, 45 (2015).
[29]E. W. K. Koh, C. H. Chiu, Y. K. Lim, Y-W. Zhang, and H. Pan, Int. J. Hydrogen Energy **37**, 14323 (2012).
[30]H. Pan, J. Phys. Chem. C **118**, 13248 (2014).
[31]H. Shi, H. Pan, Y. W. Zhang, and B. I. Yakobson, Phys. Rev. B **88**, 205305 (2013).
[32]H. Pan, Sci. Rep. **4**, 7524 (2014).
[33]D. Gao, Sh. Shi, K. Tao, B. Xia, and D. Xue, Nanoscale **7**, 4211 (2015).
[34]Y. Zhou, Q. Su, Z. Wang, H. Deng, and X. Zu, Phys. Chem. Chem. Phys. **15**, 18464 (2013).
[35]S. Wu, J. S. Ross, G.-B. Liu, G. Aivazian, A. Jones, Z. Fei, W. Zhu, D. Xaio, W. Yao, D. Cobden *et al.*, Nat. Phys. **9**, 149 (2013).
[36]G. Kresse and D. Joubert, Phys. Rev. B **59**, 1758 (1999).
[37]G. Kresse and J. Hafner, Phys. Rev. B **47**, 558 (1993).
[38]G. Kresse and J. Furthmüller, Comput. Mater. Sci. **6**, 15 (1996).
[39]J. P. Perdew, K. Burke, and M. Ernzerhof, Phys. Rev. Lett. **77**, 3865 (1996).
[40]See supplementary material at http://dx.doi.org/10.1063/1.4927286 for additional details on structural properties.
[41]J. P. Perdew, A. Ruzsinszky, G. I. Csonka, O. A. Vydrov, G. E. Scuseria, L. A. Constantin, X. Zhou, and K. Burke, Phys. Rev. Lett. **100**, 136406 (2008).
[42]P. W. Anderson, Phys. Rev. **109**, 1492 (1958).
[43]R. Skomski, *Simple Models of Magnetism* (Oxford University Press, Oxford, 2008).
[44]P. Johari and V. B. Shenoy, ACS Nano **5**, 5903 (2011).
[45]M. Gojdoš, K. Hummer, G. Kresse, J. Furthmüller, and F. Bechstedt, Phys. Rev. B **73**, 045112 (2006).
[46]M. Fox, *Optical Properties of Solids* (Oxford University Press, Oxford, 2001).
[47]T. Heine, Acc. Chem. Res. **48**, 65 (2015).